Pure & Appl. Chem., Vol. 64, No. 6, pp. 865–872, 1992.
Printed in Great Britain.

Progress in instrumentation for pulsed EPR and ENDOR spectroscopy

Jörg Forrer[1], Susanne Pfenninger[1], Bernhard Wagner[2] and Thomas Weiland[2]
[1]Laboratorium für Physikalische Chemie, Eidgenössische Technische Hochschule, CH-8092 Zürich, Switzerland.
[2]Institut für Hochfrequenztechnik, Technische Hochschule Darmstadt, D-6100 Darmstadt, Germany.

Abstract - This paper describes: (a) A self-made high speed receiver processor which increases the experimental repetition rate of time domain experiments. (b) Investigations to improve the actual excitation bandwidth of time domain EPR and ENDOR experiments. (c) Details of a pulsed ENDOR spectrometer with automatic frequency tuning and the performance of a pulsed ENDOR probehead. (d) For the first time three dimensional numerical calculations of the microwave **B**- and **E**-field distributions of a pulsed ENDOR probehead.

INTRODUCTION

The improvement of resolution and sensitivity in pulsed EPR and ENDOR experiments is still a challenge for the spectroscopist. In this contribution we report on an early design of a high speed analog signal receiver parallel digital processor orginally constructed for saturation recovery EPR (ref.1). Because of the high repetition rate of up to 200 kHz this instrument also becomes very attractive for other time domain EPR experiments like Fourier Transform (FT) EPR (ref.2), extended time electron-spin-echo-envelope modulations (ESEEM) (ref.3) and FT-EPR detected NMR (ref.4).

We then discuss the coupling of microwave resonators in terms of bandwidth and sensitivity. This is of particular importance in FT-EPR, soft ESEEM (ref.5) and FID-detected hole burning experiments (ref.6).

Details of a pulsed ENDOR spectrometer working in the frequency range between 3 and 35 MHz with pulse power up to 2.5 kW and an automatic frequency tuning loop are presented. The performance of a recently introduced pulsed ENDOR probehead (ref.7-10) with a bridged loop-gap resonator (BLGR) is demonstrated on an rf-driven ESEEM experiment (ref.6,11) which requires intense radio-frequency (rf) **B**-fields. The efficiency of the ENDOR probehead could be improved by an rf shield as confirmed by measurements and calculations.

For the first time, three dimensional microwave (mw) electromagnetic field distributions in a pulsed ENDOR probehead have been calculated. The influence of the rf shield, the rf coil, the coupling loop and all dielectrics have been included in this numerical computation.

HIGH SPEED RECEIVER PARALLEL PROCESSOR

The application of multichannel high speed receivers with sampling frequencies $f_s = 1/\Delta t$ up to 400 MHz is now common practice in FT-EPR. However, the transfer of the digitized data to a computer for data accumulation is time consuming and limits the experimental repetition rate. FT-EPR or saturation recovery experiments require a large bandwidth. This leads to a low signal-to-noise (S/N) ratio assuming sensitive EPR signal detection. The improvement of a low S/N ratio requires a large number of additions. The dynamic range D (ref.12) defines the required number of additions to achieve a desired S/N improvment of the receiver input signal.

$$D = 2\frac{(S/N)^2_{output}}{(S/N)_{input}} \qquad (1)$$

The architecture of the receiver parallel processor is shown in Fig. 1. The amplified signal is passed through a low-pass filter with a cutoff frequency f_c of $1/(2\Delta t)$ to $1/(4\Delta t)$ where Δt is the programmable sampling interval (20-200 ns). It should be noted that the design of this parallel processor was realized 15 years ago (ref.1) and that sampling intervals as short as 2.5 ns are possible with todays modern ECL electronic components. After analog-to-digital convertion (ADC) each bit of the first eight digitized data are directed into an 8 bit shift register and directed for data processing into eight parallel working processor memory boards (T_1-T_8). Each processor board consists of an arithmetic logic unit, a 128x23 RAM array and a buffer register with 3-state outputs. A 23 bit word was used yielding a wide dynamic range. The first eight data (channels) are processed and stored in address location 2^0, at the same time the second eight digitized data are shifted into a second shift register array and then directed to the parallel processor boards to be processed and stored in the incremented address location (2^1). The first processor board (T_1) processes and stores signals corresponding to channel 1,9,17. The second (T_2) handles channel 2,10 and 18 etc.. The timing between data shifting and processing is improved with two alternate working shift register arrays (Fig. 1). Parallel processing in this manner improves the experimental repetition rate by a factor of 500 - 1000 resulting in a pronounced improvement in sensitivity. The programmable address length determines the number of channels and allows the accumulation of the desired number of data points (channels). In principle, this is used to optimize the repetition rate and the spectral resolution (ref.13). The data are processed by means of adding a programmed number of decays and subtracting the same number of off-resonant background synchronous noise traces with a frequency of 100 Hz. The subtraction of these noise traces prevents fast overloading. Finally, the accumulated data may be transfered to a computer for further data handling or displayed on a CRT via address counter and time select unit (BCD to decimal decoder).

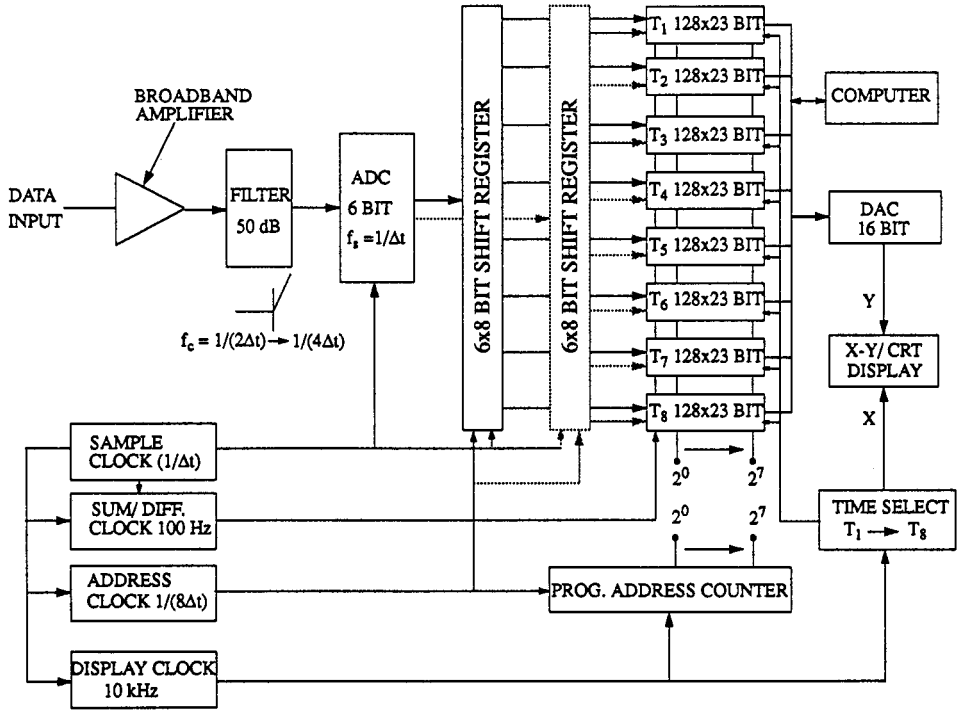

Fig. 1 Simplified block diagram of the high speed receiver parallel processor.

An application of the high speed receiver parallel processor system is given in Fig. 2 (ref.14-16) which shows saturation recovery signals of stearic acid spin label 2-(14-carboxytetradecyl)-1-ethyl-4,4-dimethyl-3-oxyzlidinoxyl (^{14}NC16) in dimyristoylphosphatidylcholine liposomes with and without cholesterol. Each of the two decays consists of $6 \cdot 10^6$ experiments that have been accumulated in 5 minutes (Δt = 20 ns, 512 channels).

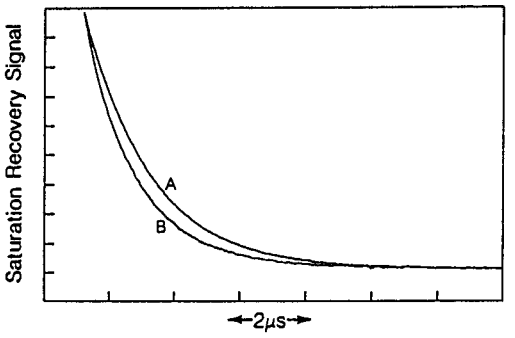

Fig. 2 Saturation recovery signal of ^{14}NC16 (0.5 mol%) in dimyristoylphosphatidyl- choline liposomes at 37°C, pH = 9.5. (A) no cholesterol, (B) with 30 mol% cholesterol (ref.15).

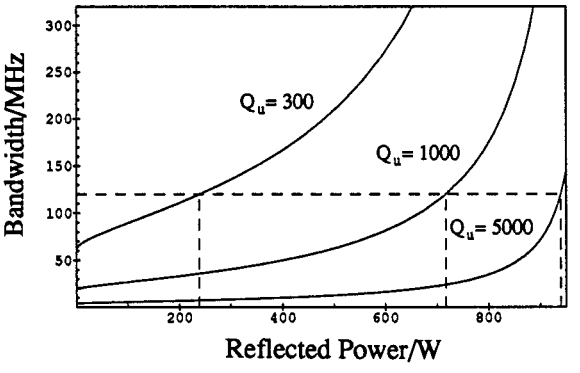

Fig. 3 Bandwidth versus reflected power for over-coupled resonators with different unloaded Q values: Q_u = 300, 1000 and 5000 (incident power: 1kW).

MICROWAVE RESONATORS

Lumped-circuit resonators have emerged as the most suitable resonator structures for time domain EPR applications (ref.7,17,18). A high filling factor and a relatively low Q value are properties of these resonators.

1. Microwave coupling

The mw power may be coupled to mw resonators by a loop (Fig. 5) or a λ/4 antenna, which both are attached (soldered) to a mw coaxial-cable (coax), or it is coupled via an iris. The coupling coefficient β is defined by

$$\beta = (1+|\Gamma|)/(1-|\Gamma|) \tag{2}$$

$$|\Gamma|^2 = P_r/P_i\,. \tag{3}$$

$|\Gamma|$ is the magnitude of the reflection coefficient, P_r is the reflected power and P_i is the incident power. The coupling coefficient β is mechanically set by the distance between the coupling loop and a high **B**-field area or by the λ/4 antenna and a high **E**-field region of the resonator. If an iris is used, β is influenced by the dimensions of the iris. The iris is placed at a position of the resonator shield with maximum current.

2. Microwave overcoupling

The usual values of the unloaded quality factor, Q_u, of these mw resonators lie between 200-2000. These values are still too high to achieve bandwidths ≥ 100 MHz at a resonant frequency of 10 GHz. To overcome this problem, overcoupling between the mw source and the resonator impedance is used (ref.19). Since overcoupling causes power reflection of part of the incident mw power, it always is a trade-off between the desired bandwidth, the Q_u value and the available mw power for the excitation of the spin system. The relation between achievable bandwidth b and reflected power P_r for 1kW incident power is given by:

$$b = \frac{f_{mw}}{Q_u}\left(1+\frac{1+\sqrt{P_r}}{1-\sqrt{P_r}}\right) \tag{4}$$

where f_{mw} denotes the mw frequency. Fig. 3 shows the bandwidth as a function of the reflected power for overcoupled mw resonators with three different Q_u values. For a bandwidth of 120 MHz and a Q_u = 5000 (TE_{102} cavity), only 60 W of mw power enters the resonator, whereas for Q_u = 300 (BLGR), 760 W mw power are available for the excitation of the sample. Hence, overcoupling is much more efficient for resonators with relatively low Q_u values.

Experiments confirm that low Q values are easy to achieve by a slight overcoupling of resonators with Q_u values between 200 - 500. Overcoupling becomes especially important at liquid Helium temperature where Q_u increases up to a factor three compared to the value at room temperature (ref.20).

PULSED ENDOR

1. Spectrometer

A block diagram of our tuned, pulsed X-band ENDOR spectrometer (ref.11,21-23) is shown in Fig. 4a.

A Varian E-Line spectrometer is extended to a computer controlled pulsed ENDOR instrument. Rf pulses are generated by an rf modulator and a pulse sequence generator with pulse lengths ≥ 0.1 μs. The rf is swept by a computer controlled rf oscillator (Wavetek 3000). Impedance matching between the pulse rf amplifier (output: 2.5 kW) and the parallel resonant circuit consisting of an rf coil and a variable vacuum capacitor (Jennings CML 8-650 pF, 5 kV) is achieved by three in series connected matched power line transformers (ref.24,25). Automatic frequency tuning is achieved by a phase control loop which consists of a phase discriminator, an rf filter, an isolation and hysteresis amplifier, and a stepper motor. An rf field strength up to 20 mT can be produced in the frequency range between 3 and 35 MHz with a pulse power of 2.5 kW. This corresponds to a field strength ten times larger than that obtained with broad band systems.

This instrumentation has been used for pulsed ENDOR experiments where high rf fields are required, as for example for liquid samples (ref.9). In such isotropic systems, echo modulations can not be generated, since in the Hamiltonian nonsecular terms are absent. In an rf-driven ESEEM experiment (ref.6,11), such terms may be created by intense rf irradiation during the mw pulse sequence. Echo modulations with a depth proportional to the square of the rf field strength are observed, if the rf irradiation is tuned to one of the nuclear transition frequencies. These modulation frequencies are related to the hyperfine coupling constants. The modulation pattern measured with rf-driven ESEEM also contains information about the number of equivalent nuclei. Rf-driven ESEEM pattern of the galvinoxyl radical in mineral oil is shown in Fig. 4c.

2. Probehead

The probehead is the main part of the spectrometer which determines the sensitivity. The resonator for pulsed ENDOR consists of a BLGR and a solenoidal flat coil that generates the rf field, and serves simultaneously as mw radiation shield (ref.9). BLGR and rf flat coil are mounted in a cylindrical copper housing representing the rf radiation shield. A longitudinal cross section of the set-up is shown in Fig. 5.

The flat coil is made by electrochemical deposition of copper on a chemically treated Teflon rod (length: 32 mm, outer diameter $\geq$ 11 mm) with the structure of the flat coil machine cut on the surface. The copper plated Teflon rod (ref.25) is then machined to produce the actual shape of the coil (Teflon wall thickness: 0.5 mm; coil dimensions: $\varnothing_{in}$ =10.5 mm, $\varnothing_{out}$ = 12 mm, length: 32 mm with 4 to 26 turns).

3. MW resonator

The recently introduced X-band BLGR (ref.7-10) has proven to be a favourable resonant structure for pulsed EPR and ENDOR experiments. It is distinguished by a high filling factor, a high rf transparency up to 200 MHz (ref.9), a high resistivity against electric break through, a large sample access (5 mm i.d.), and a low Q value which leads to suitable overcoupling conditions (Fig. 3).

A cross section at half height of the BLGR is shown in Fig. 6. The resonant structure is formed by metallic layers of 0.5-4 μm thickness on the inner and outer surface of a quartz tube ($\varnothing_{outer}$ = 6 mm, $\varnothing_{inner}$ = 5 mm, length = 4-10 mm). The metallic layer inside the quartz tube is split by two gaps parallel to the tube axis and bridged by two metallic layers on the outside. The bridged gap structure favours four high E-field areas between the outside of the metallic loop and the bridge. This structure reduces the droop of the B-field in the gap areas and also the E-field strength in the sample area. The inner loop forms the inductive part, the bridged regions the capacitive part. This structure together with the mw shield determines the resonant frequency. The mw shield either consists of a metallized quartz tube, an rf flat coil or a solenoid applied for fast field jumps. The Q value may be adjusted by varying the thickness of the metallic layers (ref.7).

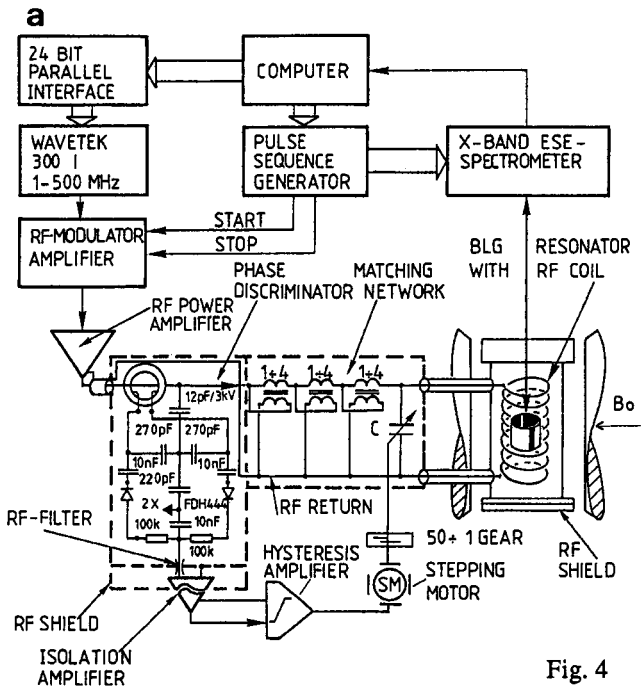

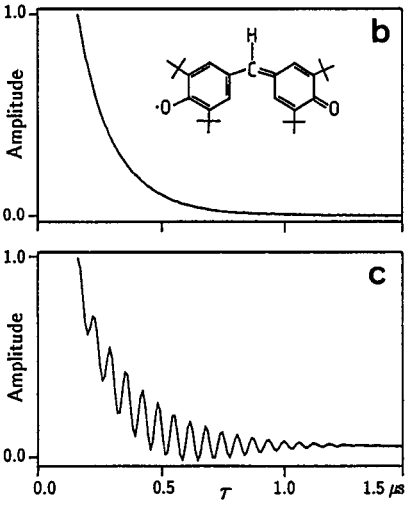

Fig. 4

a) Block diagram of the tuned, pulsed ENDOR spectrometer.
b) Two-pulse electron-spin-echo decay of the galvinoxyl radical in mineral oil (10^{-3} M), room temperature.
c) Rf-driven ESEEM pattern of the same radical, room temperature, $\omega_{rf}/2\pi = 21.307$ MHz, $B_{rf} = 11.9$ mT.

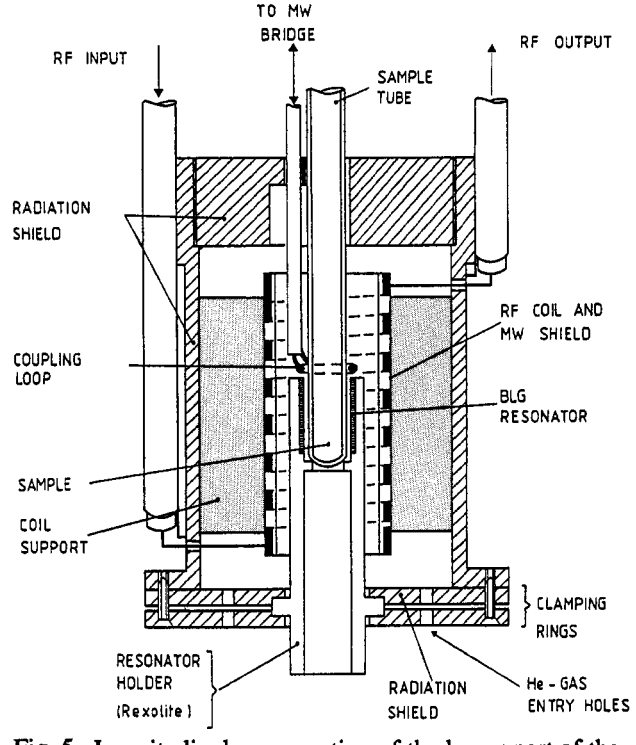

Fig. 5 Longitudinal cross section of the lower part of the pulsed ENDOR probehead with a 6.5 turn rf flat coil. Radio-frequency range: broad band: 1-200 MHz; tuned: 15-36 MHz; mw resonant frequency: 9.2 GHz; π/2 mw pulse power: 13 W (mw band-width: 40 MHz, pulse width: 20 ns).

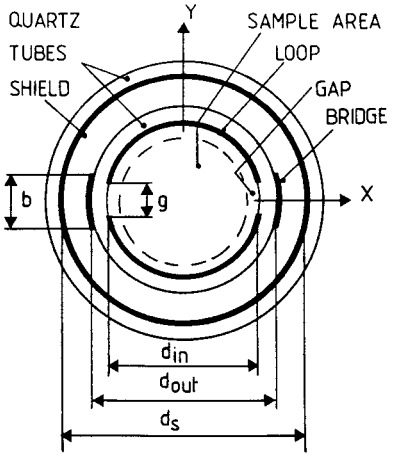

Fig. 6 Cross section of the BLGR at half height of the resonator. The defined coordinate system will be used throughout the numerical calculations. The z-axis is parallel to the resonator axis.

FIELD COMPUTATIONS

In an effort to obtain detailed information about the influence of the rf flat coil on the mw **B**- and **E**-field distributions in the sample area of the pulsed ENDOR probehead numerical computations have been carried out. The calculations are based on a special finite-difference method (ref.27-29) that solves the Maxwell equations in a consistent way. Each of these equations are transformed to equivalent matrix expressions that can be subsequently treated by matrix mathematics and suitable numerical methods for solving matrix problems.

The full size of the ENDOR probehead with rf coil or a metallic shield (Fig. 5) has been modeled in a grid of 160000 nodes with 990000 unknowns. This includes the rf shield with a diameter of 25.5 mm, the Teflon coil support, the rf flat coil with 6.5 turns, the quartz tube with the metallic BLGR structure, the Rexolite

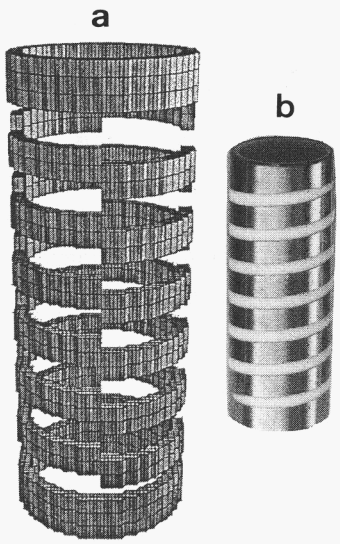

Fig. 7
a) Modeled copper rf flat coil without Teflon support tube, length: 32 mm $\emptyset_{in}$: 10 mm.
b) Photograph of the original rf flat coil.

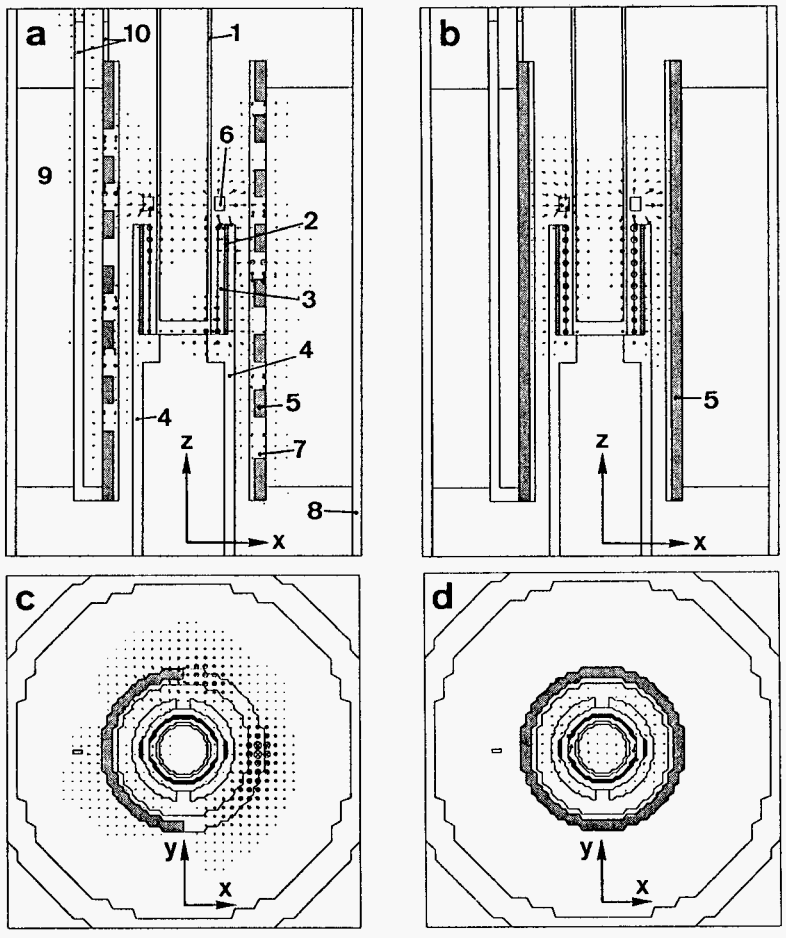

Fig. 8 **E**-field distribution in the xz and xy plane of two probeheads.
a) ENDOR set-up, the number denotes: (1) Teflon sample tube, (2) metallic layers of the BLGR, (3) resonator quartz tube, (4) Rexolite resonator holder, (5) copper rf flat coil, (6) coupling loop, (7) Teflon rf flat coil support, (8) rf copper shield, (9) Teflon support tube,(10) rf feeds terminated with 50 Ω.
b) BLGR with a solid mw shield (5)
c), d) cross section at half height of the resonant structure (a) with, (b) without rf coil.

holder of the BLGR, the Teflon sample tube, the coupling loop, and the 50 Ω coax feed to the rf coil. An example of a modeled part, the rf flat coil, is shown in Fig. 7 together with a photograph of the original coil. The pitch of the turns are realized in four steps. The discretized Maxwell equations are solved for each grid cell with the program MAFIA (ref.30) on a IBM RS 6000/320. Similar computations of the BLGR have been presented in earlier works (ref.7).

The computations show that both probeheads (with solid mw shield or with rf coil) have resonant frequencies at 6 and 9.2 GHz. In an attempt to shift the frequencies the modeled bridge width b (Fig. 6) of the BLGR was reduced from 2 to 1.5 mm. The lower frequency of 6 GHz was not affected by this change but the higher was shifted from 8 to 9.2 GHz. With an rf coil the upper frequency is down shifted by about 30 MHz in contrast to a solid mw shield. The **E**- and **B**-field distributions in the xz and xy planes of these two resonators are presented in Fig. 8 and Fig. 9, respectively. The xy plane is placed at half height of the resonator. The **E**-field distribution in the ENDOR probehead and the BLGR with a solid mw shield are quite different from each other (Fig. 8). The **E**-field penetrates through the spaces between the windings of the rf coil and has also a finite amplitude outside the rf coil.

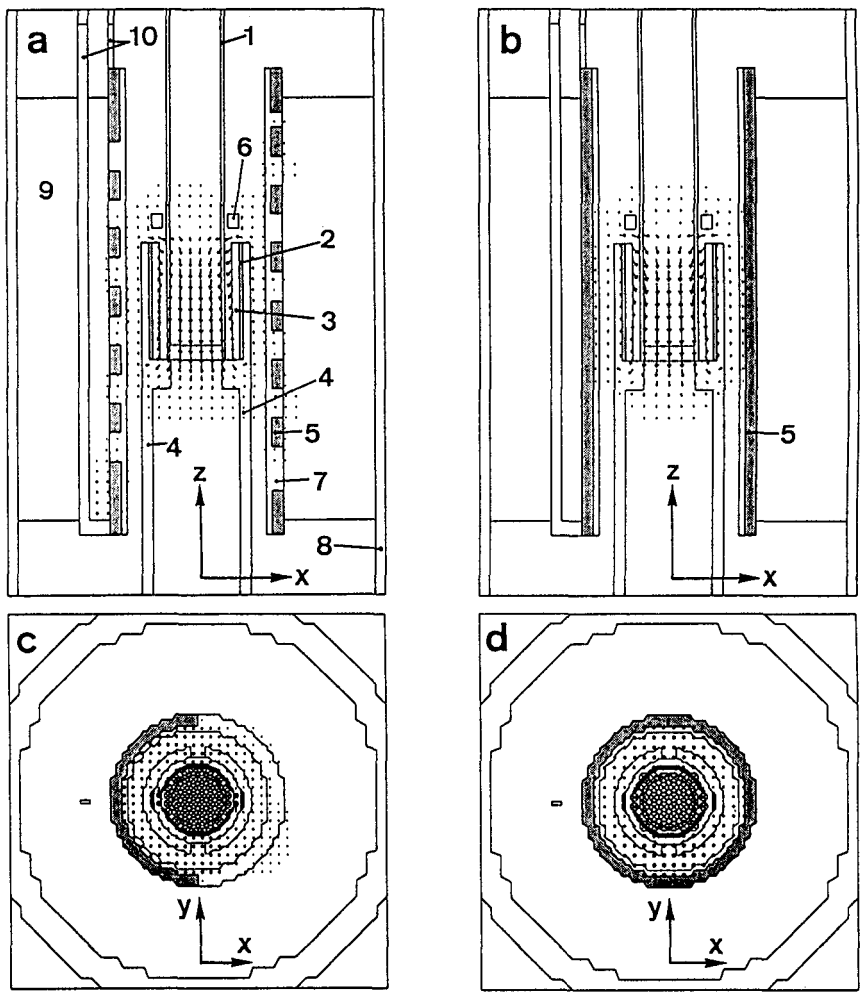

Fig. 9 B-field distribution in the xz and xy plane of two probeheads.
a) ENDOR set-up (maximum arrow: 19.1 mT)
b) BLGR with a solid mw shield (5), (maximum arrow: 19.5 mT)
c), d) cross section at half height of the resonant structure, (a) with and (b) without rf coil.

The dimensions of the housing result in no additional modes. The E-field strength between the coupling loop and the metallic layers of the BLGR is very high. This may be critical for a too strongly overcoupled BLGR where the coupling loop is very close to the resonator.

Fig. 9 shows for both cases a very homogeneous **B**-field distribution in the sample area but not in the coupling loop region. A pronounced deviation of the direction of the **B**-field vectors towards the bridged gap area (along x) in the xy plane has no influence on the transition probability, if the static field is perpendicular to the xz plane. It is remarkable that the homogeneity in the xy plane (Fig. 9c,b) is not influenced by the semi-open mw shield represented by the rf coil.

Acknowledgement

The support and advice of Prof. Arthur Schweiger are much appreciated. We thank Angelina Zuelli for the drawing the schematics. We are grateful to Prof. James S. Hyde and Dr. Jun-Jie Yin from the National Biomedical ESR Center of the Medical College of Wisconsin for the copyright of Fig. 2. This research has been supported by the Swiss National Science Foundation.

REFERENCES

1. J. Forrer, R.C. Wubben and J.S. Hyde, *Bull. Mag. Res. 2,* 441 (1980).
2. J. Gorcester, G.L. Millhauser and J.H. Freed in L. Kevan, M.K. Bowman (eds.), *Modern Pulsed and Continuous Wave Electron Spin Resonance*, Wiley, New York, 119-194 (1990).
3. A. Schweiger, L. Braunschweiler, J.-M. Fauth and R.R. Ernst, *Phys. Rev. Lett. 54,* 1241-1244 (1985).
4. Th. Wacker and A. Schweiger, *Chem. Phys. Lett. 186,* 27-34 (1991).
5. A. Schweiger, C. Gemperle and R.R. Ernst, *J. Magn. Reson. 86,* 70-81 (1990).
6. A. Schweiger, this conference.
7. S. Pfenninger, J. Forrer, A. Schweiger, and Th. Weiland, *Rev. Sci. Instrum. 59,* 752-760 (1988).
8. J. Forrer, S. Pfenninger, A. Schweiger, and Th. Weiland, *in Magnetic Resonance and Related Phenomena, Proceedings of the XXIVth Congress Ampere, Poznan, Poland 1988* (Elsevier Science, New York, 1989) 919-924.
9. J. Forrer, S. Pfenninger, J. Eisenegger, and A. Schweiger, *Rev. Sci. Instrum. 61,* 3360-3367 (1990).
10. S. Pfenninger, J. Forrer, A. Schweiger, and Th. Weiland, *Phys. Med. V,* 203-212 (1989).
11. H. Cho, S. Pfenninger, J. Forrer, and A. Schweiger, *Chem. Phys. Lett. 180,* 198-206 (1991).
12. R.R. Ernst, *J. Magn. Reson. 4,* 280-296 (1971).
13. R.R. Ernst, G. Bodenhausen, and A. Wokaun, *Principles of Nuclear Magnetic Resonance in One an Two Dimensions,* Clarendon Press, Oxford (1987).
14. J.-J. Yin, J.B Feix and J.S. Hyde, *Biophys. J. 58,* 713-720 (1990).
15. J.-J. Yin, *Thesis, National Biomedical ESR Center, Medical College of Wisconsin* (1987).
16. J.S. Hyde,J.-J. Yin, J.B. Feix, and W. L. Hubbell, *Pure & Appl. Chem. 62,* 255-260 (1990).
17. C. Bock, M. Mehring, H. Seidel, and H. Weber, *Bull. Mag. Res. 2,* 421-422 (1980).
18. W. Froncisz and J.S. Hyde, *J. Magn. Reson. 47,* 515-521 (1982).
19. C.P. Poole, *Electron Spin Resonance. A Comprehensive Treatise on Experimental Techniques* (Interscience, New York, 1983).
20. S. Pfenninger, J. Forrer, A. Schweiger, B. Wagner and Th. Weiland, to be published.
21. J. Forrer, *Bull. SEV/VSE 75,* 1264-1267 (1984).
22. J.-M. Fauth, A. Schweiger, L. Braunschweiler, J. Forrer, and R.R. Ernst, *J. Magn. Reson. 66,* 74-85 (1985).
23. J.-M. Fauth, *Thesis ETH, No. 8645* (1988).
24. J. Forrer, A. Schweiger, and Hs.H. Günthard, *J. Phys. E: Sci. Instrum. 10,* 470-473 (1977).
25. K. Gruber, J. Forrer, A. Schweiger, and Hs.H. Günthard, *J. Phys.E: Sci. Instrum. 7,* 569-574 (1974).
26. Werner Flühmann AG, 8600 Dübendorf, Switzerland.
27. Th. Weiland, *AEU Electron. Commun. 31,*116-120 (1977).
28. Th. Weiland, *Part. Accel. 15,* 245-292 (1984).
29. Th. Weiland, *Part. Accel. 17,* 227-242 (1985).
30. MAFIA-electromagnetic design code; available from Th. Weiland, University Darmstadt, D-6100 Darmstadt, Germany.